Nuclear Instruments and Methods in Physics Research B 407 (2017) 97–109

Contents lists available at ScienceDirect

Nuclear Instruments and Methods in Physics Research B

journal homepage: www.elsevier.com/locate/nimb

How the choice of model dielectric function affects the calculated observables

Maarten Vos [a,*], Pedro L. Grande [b]

[a] Electronics Materials Engineering, Research School of Physics and Engineering, Australian National University, Canberra, ACT, Australia
[b] Ion Implantation Laboratory, Instituto de Física, Universidade Federal do Rio Grande do Sul, Av. Bento Goncalves, 9500, CP 15051, CEP 91501-970, Porto Alegre, RS, Brazil

ARTICLE INFO

Article history:
Received 27 April 2017
Received in revised form 22 May 2017
Accepted 30 May 2017

Keywords:
Dielectric function
Inelastic mean free path
Ion stopping
Reflection electron energy loss spectroscopy

ABSTRACT

It is investigated how the model used to describe a dielectric function (i.e. a Mermin, Drude, Drude–Lindhard, Levine–Louie with relaxation time dielectric function) affects the interpretation of a REELS experiment, the calculation of the electron inelastic mean free path as well proton stopping and straggling. Three dielectric functions are constructed that are based on different models describing a metal, but have identical loss functions in the optical limit. A loss function with the same shape, but half the amplitude, is used to derive four different model dielectric functions for an insulator. From these dielectric functions we calculate the differential inverse mean free path, the mean free path itself, as well as the stopping force and straggling for protons. The similarity of the underlying physics between proton stopping, straggling and the electron inelastic mean free path is stressed by describing all three in terms of the differential inverse inelastic mean free path. To further highlight the reason why observed quantities depend on the model dielectric function used we study partial differential inverse inelastic mean free paths, i.e. those obtained by integrating over only a limited range of momentum transfers. In this way it becomes quite transparent why the observable quantities depend on the choice of model dielectric function.

1. Introduction

Many processes, in particular the interaction of charged particles with matter, can be described in terms of the dielectric function $\epsilon(\omega,q)$ with q the momentum and ω the energy transfer. Unfortunately $\epsilon(\omega,q)$ is generally unknown although it can be measured directly in a transmission electron energy loss experiment [1,2] (or inelastic X-ray scattering experiment [3]) or calculated from first principle [4]. When this information is not available one has to use model dielectric functions. In that case only a limited number of parameters are required to obtain the dielectric function everywhere in (ω,q) space. Parameters for the model are usually determined by fitting the Energy Loss Function $\mathrm{Im}[-1/\epsilon(\omega,q)]$ at $q=0$ (from now on referred to as ELF) to optical data, which are much more widely available [5]. Subsequently, one can then calculate frequently used quantities such as the electron inelastic mean free path (IMFP) [6] or ion stopping and straggling from the dielectric function by a (weighted) integration of the loss function over (ω,q) space [7]. The results of these calculations are only valid if the model, describing how the dielectric function varies away from $q=0$, is correct. Here we want to study systematically how the outcome of such calculations depends on the model used.

For this purpose we construct different model dielectric functions that coincide at $q=0$. Then we calculate the aforementioned observables as well as the differential inelastic inverse mean free path (DIIMFP), the central quantity in REELS (Reflection Electron Energy Loss Spectroscopy). Such an approach will obviously show the differences of the calculated quantities for the different models, but it is often more difficult to pinpoint the origin of these differences. In all cases the calculated quantity is obtained by a weighted integration of the loss function over all accessible q values. To gain insight in the nature of the differences we integrate over only a fraction of allowed q values, and see for what range of q values the contribution to the calculated quantity of the models differ.

The main aim of this paper is to get some insight in what the consequences are of adoption one of the available model dielectric functions for the interpretation of their experiment, and under what condition this assumption is crucial for the outcome of the derived parameter(s), in particular the differential inverse electron mean free path (DIIMFP) which relates to REELS experiments, the

* Corresponding author.
E-mail address: maarten.vos@anu.edu.au (M. Vos).

http://dx.doi.org/10.1016/j.nimb.2017.05.064
0168-583X/

IMFP in electron spectroscopy and ion stopping and straggling. The approach described will highlight the similarity of the underlying physics of the electron IMFP and ion stopping and straggling.

In the context of the IMFP of water many issues explored here where recently discussed by Shinotsuka et al. [8]. The work of Nikjoo et al. [9] describes the state-of-the-art of our knowledge of the interaction of charged particles with matter in the context of medical physics.

2. Model dielectric functions

2.1. Metals

Here we present briefly the model dielectric functions we will be using. Most of them have been described extensively in the literature before, e.g. see Ref. [9–13].

The first one is the Drude dielectric function $\epsilon^{\mathrm{D}}(\omega,q)$ with $\epsilon_1^{\mathrm{D}}(\omega,q)$ and $\epsilon_2^{\mathrm{D}}(\omega,q)$ the corresponding real and imaginary part:

$$\epsilon_1^{\mathrm{D}}(\omega,q)=\epsilon_b-\sum_i\frac{A_i(\omega^2-\omega_i(q)^2)}{(\omega^2-\omega_i(q)^2)^2+\Gamma_i^2\omega^2} \tag{1}$$

$$\epsilon_2^{\mathrm{D}}(\omega,q)=\sum_i\frac{A_i\Gamma_i\omega}{(\omega^2-\omega_i(q)^2)^2+\Gamma_i^2\omega^2} \tag{2}$$

here A_i (in units of (energy)^2) relates to the density of electrons with binding energy ω_i. Γ_i determines the width of the excitation. ϵ_b is the background dielectric constant due to the polarizability of the core electrons. Such a model dielectric function was used for the interpretation of REELS experiments by Tung et al. [14], Kwei et al. [15] and Werner et al. (e.g. [16]). The energy of oscillator i can depend on q (dispersion). This dependence will be assumed here to have a simple form (using atomic units):

$$\omega_i(q)=\omega_i(0)+\alpha_i\frac{q^2}{2} \tag{3}$$

but more complex dependencies (e.g. full dispersion [17]) could be used as well. The case of $\alpha_i=1$ is often referred to as 'free-electron dispersion'. For deeper levels α_i is often chosen much smaller than 1. For metals there is one component (representing the conduction electrons) with $\omega_i(0)=0$. For a free-electron metal this is the only component and the loss function $\mathrm{Im}[-1/\epsilon(\omega,0)]$ has then a maximum at $\sqrt{A_1}$. Such a free electron plasma will have, away from $q=0$, a maximum in $\mathrm{Im}[-1/\epsilon(\omega,q)]$ at $\sqrt{A_1+\omega_1(q)^2}$. The dispersion of this peak is thus different from a free electron dispersion, even with $\alpha_1=1$. If there is more than one component in the dielectric function then different components will 'repel' each other and peak positions are somewhat from $\sqrt{A_i+\omega_i(q)^2}$ [11].

A second model is often referred to as the Drude–Lindhard (DL) model [18]. Here ϵ^{DL} is defined in terms of $1/\epsilon(\omega,q)$ rather than $\epsilon(\omega,q)$ itself:

$$\mathrm{Im}\left[\frac{-1}{\epsilon^{\mathrm{DL}}(\omega,q)}\right]=\sum_i C_i\frac{\omega\Gamma_i\omega_i(0)^2}{(\omega^2-\omega_i(q)^2)^2+\omega^2\Gamma_i^2} \tag{4}$$

and for the real part:

$$\mathrm{Re}\left[\frac{1}{\epsilon^{\mathrm{DL}}(\omega,q)}\right]=1+\sum_i C_i\frac{(\omega^2-\omega_i(q)^2)\omega_i(0)^2}{(\omega^2-\omega_i(q)^2)^2+\omega^2\Gamma^2} \tag{5}$$

In the context of REELS such an approach is used e.q. in the QUASES package [19,20]. $\omega_i(q)$ is again defined as in Eq. (3) but now $\alpha_i=1$ implies that a peak disperses indeed in the same way as a free electron. There is no interaction between different oscillators, as there is in the Drude case, as now the dielectric function is defined in terms of the loss function itself.

For a free electron metal the DL dielectric function is at $q=0$ equivalent to the Drude dielectric function if $C_1=1$ and $\omega_1^{\mathrm{DL}}=\sqrt{A_1}$, but away from $q=0$ their dispersion will differ somewhat. For a metal $\mathrm{Re}\left[\frac{1}{\epsilon^{\mathrm{DL}}(0,0)}\right]$ should correspond to 0, as DC fields are completely screened (i.e. $\epsilon_1(0,0)=\infty$). This implies that $\sum_i C_i=1$.

These loss functions have their roots in classical physics. Lindhard derived, based on quantum physics, a dielectric function for a free electron gas $\epsilon^{\mathrm{L}}(\omega,q)$ [21] (see appendix for details). Here the loss function consists of a delta function (describing collective excitations, or 'plasmons') and a continuous part (describing single-particle excitations). Mermin added relaxation time to the Lindhard dielectric function which transforms the delta function to a peak with finite width [22]:

$$\epsilon^{\mathrm{M}}(\omega,q)=1+\frac{(1+i\Gamma/\omega)(\epsilon^{\mathrm{L}}(\omega+i\Gamma,q)-1)}{1+i\Gamma/\omega[\epsilon^{\mathrm{L}}(\omega+i\Gamma,q)-1]/[\epsilon^{\mathrm{L}}(0,q)-1]} \tag{6}$$

Abril et al. used a sum of Mermin loss functions to fit a optical data [23] or REELS data (e.g. [24]) to describe the proton stopping. Denton et al. used the Mermin dielectric function to calculate the electron inelastic mean free path [25]. Da et al. used a large number of positive and negative Mermin oscillator to fit the ELF of Cu and calculate its inelastic mean free path [26]. At $q=0$ the Mermin loss function coincides with the DL loss function with the same parameters. The Mermin loss function has dispersion 'build in' and away from $q=0$ the width of peak in $\mathrm{Im}[-1/\epsilon(\omega,q)]$ increases and becomes much larger than the width of the corresponding DL Loss function (see e.g. [27]). In this paper we will consider a simple model dielectric function consisting of two components. One component causes a peak in the ELF function at 15 eV. The second component corresponds to a peak at 80 eV. This model could be seen as a very crude model of Al where the first peak corresponds to the free-electron plasmon peak, and the second peak is due to the (combined) 2p and 2s electrons. The coefficients of these components are shown in Table 1 and the loss function and ϵ_1, ϵ_2 are reproduced in Fig. 1. The coefficients are chosen such that the ELF (Energy Loss Function at $q=0$) of all three model dielectric functions are identical.

2.2. Insulators

In an insulator the band gap has the effect of moving the loss features to higher energies. However, the dielectric function should remain compliant with sum rules, e.g. the Bethe sum rule:

$$\frac{1}{2\pi^2}\int_0^\infty\omega'\mathrm{Im}\left[\frac{-1}{\epsilon(\omega',0)}\right]d\omega'=N, \tag{7}$$

with N the number of electrons per unit volume. When using the DL or Mermin model, the shift of the loss function to higher energy due to band gap means that its area, and hence the coefficient(s) C_i, should decrease in order to comply with the sum rule. Hence for an insulator $\sum_i C_i<1$. This has also as a consequence that $\mathrm{Re}[1/\epsilon(0,0)]$ has values between 0 and 1, and hence $\epsilon_1(0,0)$ is finite and larger than 1 as required for an insulator.

An insulator with a loss function with a peak at the same energy as the loss function of a metal will thus have a lower electron density. We constructed 4 model loss functions with half the electron density of our metal loss function for simplicity, but with the peaks in the ELF at the same energy loss position (and the same width). The values of the parameters used are given in Table 2. To get half the electron density within the Drude model one has to halve the A_i parameters. To retain the same peak position one has to increase

Table 1
Three different dielectric function (Drude, Drude Lindhard and Mermin), all with (virtually) the same ELF, shown in the left panels of Fig. 1.

	A_i, C_i	ω_i (eV)	γ_i (eV)	α_i
Drude	245	0	1	1
	600	76	1	1, or 0.1
D–L	0.9	15	1	1
	0.1	80	1	1 or 0.1
Merm.	0.9	15	1	–
	0.1	80	1	–

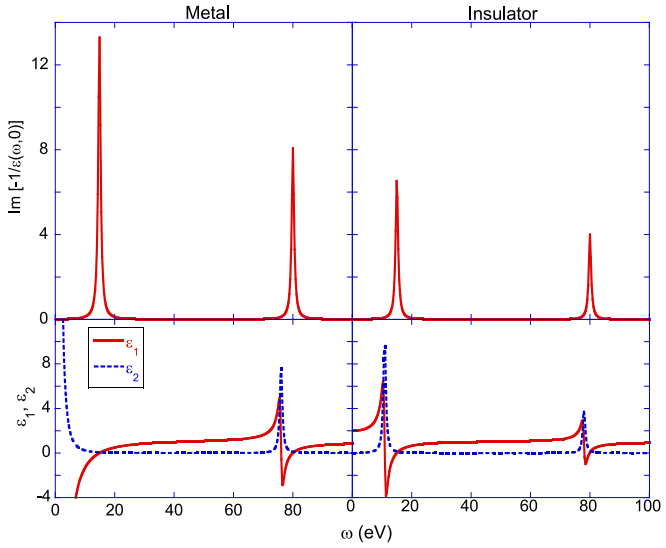

Fig. 1. The ELF (top) and ϵ_1, ϵ_2 (bottom) for our model dielectric functions for a metal (left) and an insulator (right).

the values of ω_i , in agreement with the fact that there are no free electrons (i.e. $\omega_i \neq 0$) in an insulator. For the Drude and Mermin model one has to halve the values of C_i.

The derivation of the Lindhard loss function (on which the Mermin one is based) assumes a free electron gas, and its use to describe an insulator is thus highly questionable. Levine and Louie derived a loss function based on quantum physics for an insulator (ϵ^{LL}) by transforming the energy scale according to $\omega \rightarrow \sqrt{(\omega^2 + U^2)}$ with U a parameter that is related to the gap [28] (see appendix for full expressions). It reverts to the Lindhard function when $U \rightarrow 0$. Archubi and Arista studied the effect of the U parameter on the stopping, inelastic mean free path and straggling for electrons, positrons and protons using the ϵ^{L} (or equivalently, ϵ^{LL} with $U = 0$) and ϵ^{LL} dielectric function with $U \neq 0$ [29]. Here we add a relaxation time to this function by replacing ϵ^{L} in Eq. (6) by ϵ^{LL} and refer to the resulting dielectric function as ϵ^{MLL} (Mermin–Levine–Louie). Using this approach one has $\sum_i C_i^{MLL} = 1$ as a boundary condition, but by choosing the appropriate ω_i and U values one can obtain again the same loss function in the optical limit. For details see Ref. [12].

The above-defined dielectric functions are by no means the only ones. Model dielectric functions have been developed over decades and which is the most appropriate one will depend to some extent on the phenomena one wants to describe. Penn and co-workers used the Lindhard dielectric function itself for the extraction of the electron inelastic mean free path from optical data [6,30]. The dispersion relation (Eq. (3)) can be replaced by a 'full dispersion model' [17]. The width Γ_i in the Drude or Drude–Lindhard model can be taken to depend on q [31–33]. Burke and Chantler developed a scheme that makes it possible to derive the width from the dielectric function itself [34]. The method described here could be easily applied to these and other dielectric functions to gain insight in the consequence of the assumptions made for mean free path, stopping and straggling.

3. The DIIMFP in REELS experiments

In a REELS experiment a collimated beam of electrons with well-defined energy E_0 and momentum $\boldsymbol{k}_0$ impinges on a surface and one measures the energy of the electrons reflected from this surface. In practice the E_0 values used vary from several hundred eV to 40 keV. Consider such a REELS experiment and, for the simplicity of the argument, we assume first that surface excitations are absent. The REELS spectrum can then be described in terms of the DIIMFP (Differential Inverse Inelastic Mean Free Path). The DIIMFP at energy ω is proportional to the probability that an electron loses a quantum ω of energy per unit length traveled. The REELS spectrum is then proportional to the DIIMFP (due to trajectories with only one inelastic scattering event) plus contributions proportional to the $(N-1)$ times self-convolution of the DIIMFP (due to trajectories with N inelastic scattering events). In reality surface excitations are present and near the surface the probability of exciting bulk plasmons is reduced. The picture described above has to be modified and different methods how to analyze a REELS measurement have been given in the literature [19,35].

Table 2
The model dielectric function of an insulator in either the Drude, DL, Mermin, and MLL model, based on 2 oscillators. The oscillators were chosen such that their ELF in the optical limit is identical (right panel of Fig. 1). For the D–L and Mermin models: $\sum C_i = 0.5$. For the MLL model $\sum C_i = 1$.

	A_i, C_i	ω_i (eV)	γ (eV)	α_i	U (eV)
Drude	122	10.5	1	1	–
	300	78.1	1	0.1, 1	–
D–L	0.45	15	1	1	–
	0.05	80	1	0.1, 1	–
Merm.	0.45	15	1	–	–
	0.05	80	1	–	–
MLL	0.947	10.3	1	-	11.0
	0.053	79.3	1	–	11.0

Here we assume that one has successfully retrieved the DIIMFP from a REELS experiment (a non-trivial task) and concern us with the question how to extract the dielectric function corresponding to this DIIMFP. The (bulk) DIIMFP $W_b(\omega, E_0)$ is related to the dielectric function as [36]:

$$W_b(\omega,E_0) = \frac{2}{\pi m v^2}\int_{q_-}^{q_+}\frac{dq}{q}\mathrm{Im}\left[\frac{-1}{\epsilon(\omega,q)}\right] = \frac{1}{\pi E_0}\int_{q_-}^{q_+}\frac{dq}{q}\mathrm{Im}\left[\frac{-1}{\epsilon(\omega,q)}\right] \quad (8)$$

with E_0 the incoming energy. The mass m in Eq. (8) is the mass of the target electrons, and v the velocity of the projectile. Only if the mass of the projectile M equals that of a target electron can we replace $2/mv^2$ by $1/E_0$. When working in atomic units $m = 1$ and can be omitted from Eq. (8). The limits of integration $q_\pm$ are a consequence of conservation of energy and momentum, as explained in Fig. 2a) and are given by (velocities are assumed non-relativistic throughout this paper):

$$q_\pm = \sqrt{2ME_0} \pm \sqrt{2M(E_0-\omega)}. \quad (9)$$

In particular q_- is pivotal for the outcome of this integral. It depends both the incoming energy E_0 and the energy loss ω.

If one wants to obtain the dielectric function from a REELS experiment one *assumes* a model function and determines the parameters for which it describes the measured DIIMFP best. The results are then usually presented by plotting the ELF i.e. the loss function at $q = 0$ for the dielectric function that described the measurement best. Here we work the other way around, and see how the DIIMFP for a given ELF depends on the model dielectric function used. For this we consider the different model dielectric functions of Table 1, and calculate the DIIMFP for several incoming energies.

In order to get some insight in what is happening we evaluate also 'partial' DIIMFP integrals i.e. integrate only over slices of q, i.e from 0 to 0.1 a.u. from 0.1 to 0.2 a.u etc. up to from 0.9 to 1 a.u. There is of course only a contribution to the integral if $q > q_-$. We also evaluate the integral with the proper boundaries (Eq. (9)). In this way we can investigate the contributions to the DIIMFP of scattering events with different q values.

The results for the Drude model are given in Fig. 3(a) with α_2 describing the dispersion for the deeper level taken to be 0.1. It is customary to take α much smaller than 1 for deeper levels in REELS analysis using the Drude model (see e.g. [16,37]).

There are quite a few things to point out here. Firstly, there is almost no intensity in the partial DIIMFP obtained by integrating

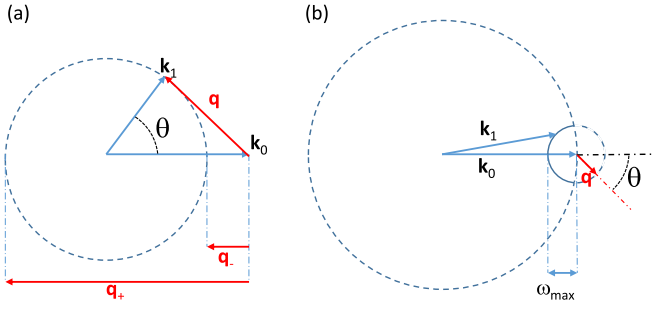

Fig. 2. In (a) we show the kinematics at constant energy loss ω. The transferred momentum q is the difference in momentum particle before ($|k_0| = \sqrt{2ME_0}$) and after ($(|k_1| = \sqrt{2M(E_0-\omega)})$) the energy loss event and varies from $q_- = |k_0| - |k_1|$ for $\theta = 0^\circ$ to $q_+ = |k_0| + |k_1|$ for $\theta = 180^\circ$. In (b) we show the kinematics at constant magnitude of $\boldsymbol{q}$. The largest energy loss is now (for $\theta = 180^\circ$) $\omega_{max} = k_0^2/2M - (k_0 - q)^2/2M \simeq q v_0$. The dashed part of the small circle corresponds to energy gain, and can not be accessed.

q from 0 to 0.1 a.u. for the measurement with $E_0 = 0.3$ keV. The 15 eV level is visible for $q > 0.1$ a.u. and the deeper level only for $q > 0.6$ a.u. Clearly the minimum momentum transfer for these excitation (which occurs at $\theta = 0$) is larger than 0.1 a.u. This is illustrated in Fig. 4 which shows q_- together with the dispersion of the plasmon. The dispersion curve crosses the q_- curve, and the oscillator will only contribute strongly to the partial DIIMFP for those q values where the q_- curve is to the right of the dispersion curve. If this is not the case then there can still be a little intensity in the partial DIIMFP because of the wings of the peak in the loss function extending towards zero energy loss. For the 80 eV level the corresponding q_- values are much larger and it contributes significantly at $E_0 = 0.3$ keV only for q values above 0.7 a.u.

At 2.5 keV the 15 eV level is already observed in the $q = 0 - 0.1$ a.u. plot and the deeper level is observed from $q = 0.2$ onwards. At 40 keV both levels contribute already to the lowest momentum bin.

The top panels of Fig. 3a shows the total DIIMFP and the contribution of the DIIMFP up to 1 a.u. In all cases the total contribution to the outer oscillator is almost the same as the contribution from 0 to 1.0 a.u. This is not true for the deeper level. At 300 eV the majority of its contribution originates from collisions with $q > 1.0$ a.u. The larger E_0 the more the DIIMFP resembles the optical ELF. This is because with increasing E_0 an increasing fraction of the DIIMFP intensity is generated by scattering events with small q values, where dispersion plays only a minor role.

For the Drude model the $\omega = 15$ eV feature is hardly affected by dispersion, although its dispersion coefficient α is taken to be 1. This is because the dispersion of the Drude dielectric function follows $\sqrt{A_1 + \omega_1(q)^2}$ and small changes of $\omega_1(q)$ away from 0 will hardly influence the result of this expression. The deeper level is affected by dispersion quite strongly (a clear tail extending to higher energy losses is seen for the 80 eV feature in the DIIMFP), in spite of the fact that α was taken to be 0.1 for the 80 eV level. This can be understood as its contribution comes from larger q values and the effect of the larger q values on $\alpha q^2/2$ term is more important than the reduced α value. This is in particularly obvious for the $E_0 = 300$ eV case.

A similar picture, but now for the DL model, is shown in Fig. 3b. Again α_2 was taken to be 0.1. Now the dispersion of the 15 eV level is much more pronounced in the partial DIIMFP, and the broadening of the 15 eV and 80 eV level in the total DIIMFP is now comparable. Again the reduction in α_2 is compensated by the larger q values that contribute to the DIIMFP for the deeper level.

In Fig. 3c we show a similar plot for the Mermin dielectric function. Now dispersion is 'built-in' and there is no adjustable α parameter. The dispersion is close to DL for the 15 eV level but the peak shows now significant additional broadening away from $q = 0$, with some intensity extending almost all the way to $\omega = 0$. As we will see later this tail is crucial for the IMFP at low E_0 values. The dispersion of the deeper level is in the Mermin model of similar magnitude to the dispersion of the 15 eV level. As the contribution to the DIIMFP from the deeper level comes mainly from contributions at larger q value, it appears much more broadened in the total DIIMFP, especially for low E_0 values where it is almost completely washed out. At higher energy (2.5 keV and 40 keV) a clear peak remains but its maximum intensity, relative to the 15 eV feature, is much reduced compared to the intensity ratio in the optical ELF (see Fig. 1). A very similar washing out of the deeper feature would be seen in the Drude and DL model if one takes $\alpha_2 = 1$.

These model calculations demonstrate an intrinsic problem when trying to retrieve the optical ELF from measured REELS data. Here one obtains from the measurement (after a non-trivial analy-

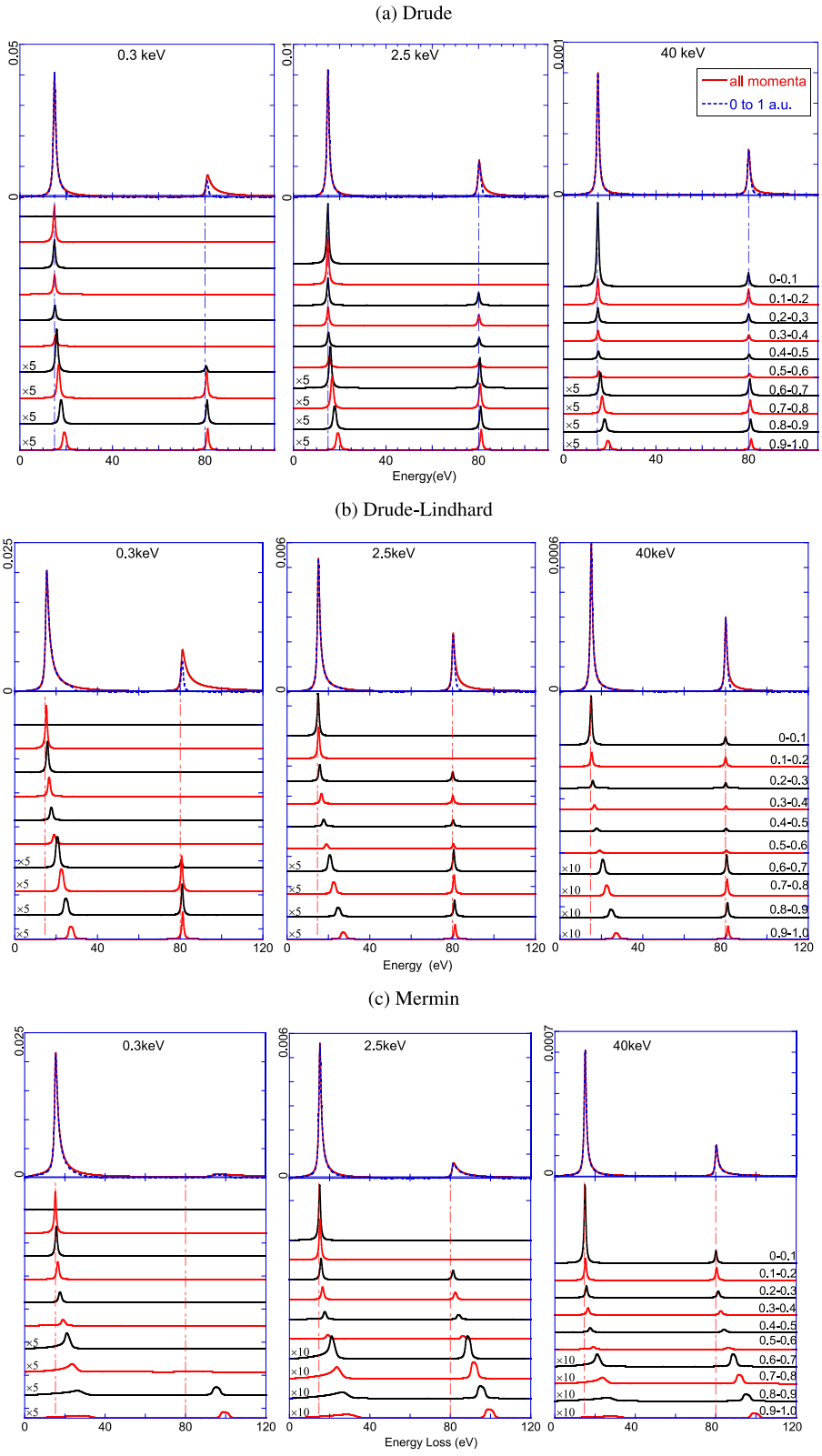

Fig. 3. Total and partial DIIMFP for (A) the Drude model, (B) DL and (C) the Mermin model. The top panels show the total DIIMFP (full line) and the partial DIIMFP integrated from 0 to 1 a.u (dashed). The lower panel shows the partial DIIMFP for 0.1 a.u. wide slices, as indicated in the right panel. These graphs are offset vertically for clarity.

sis is applied) an estimate from the DIIMFP. Retrieving the optical ELF from this DIIMFP is then model dependent, and will affect the optical ELF obtained, especially for larger ω and smaller E_0 values. One could try to exploit this property to test the dispersion model used by comparing the obtained ELF from low energy REELS data with those obtained from transmission EELS measurements or

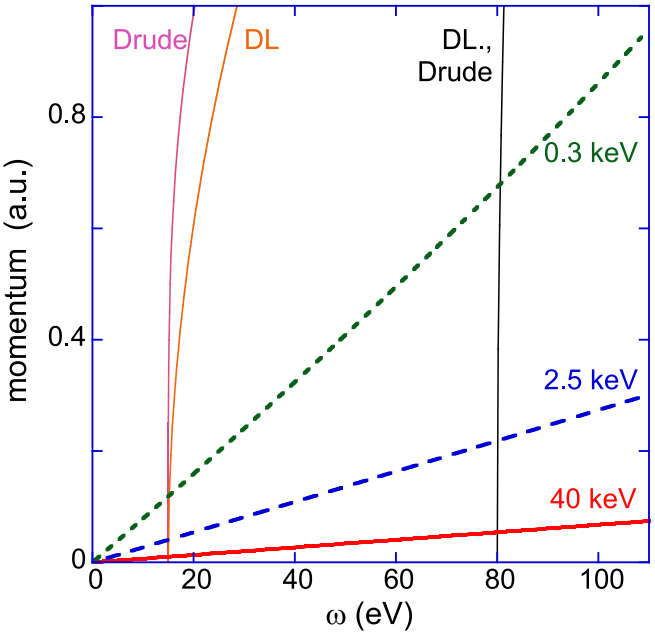

Fig. 4. The lower limit of the integration used to calculate the DIIMFP for incoming energies of 0.3, 2.5 and 40 keV as a function of energy loss, as well as the dispersion of both oscillators used for the DL model with $\alpha = 1$ for the 15 eV level and 0.1 for the 80 eV one.

higher energy REELS experiments, and check for what model the best agreement is obtained, but this has not been attempted to our knowledge.

For clarity we took the deeper level at quite a high binding energy (80 eV). Usually 40 eV is more typical for the position of the deeper levels in a REELS derived DIIMFP. Then these effects are still present, but less severe. However, it is quite likely that difficulties in interpreting REELS measurements [38] have at least in part its origin here.

4. Electron inelastic mean free path

If one integrates the DIIMFP (Eq. (8)) over all possible energy losses one obtains the inverse mean free path $1/\lambda$ i.e. the probability that an inelastic event happens per unit length. At lower energies it is essential that one specifies relative to what level (Fermi level, vacuum level or the bottom of the conduction band) the kinetic energy is defined. Moreover, at low energies it is also essential that one takes into account that the allowed final states of the projectile are affected by the Pauli exclusion principle. To keep things simple we will work here in the first Born approximation and not consider complications due to exchange and the effect of Pauli's exclusion principle on screening, see e.g. Ref. [39,40] for a discussion of these effects. We define the kinetic energy relative to the bottom of the (valence) band and take into account Pauli's exclusion principle (i.e. the final state of the projectile should be outside the occupied Fermi sphere. This means the remaining energy should be larger than E_f or alternatively: $|k_1| = |\boldsymbol{k}_0 - \boldsymbol{q}| > k_f$ [41]) one obtains for metals (see Fig. 5):

$$1/\lambda = \int_0^{E_0-E_f} W_b(\omega, E_0)d\omega = \int_0^{E_0-E_f} \frac{d\omega}{\pi E_0}\int_{q_-}^{q_+}\frac{dq}{q}\,\mathrm{Im}\left[\frac{-1}{\epsilon(\omega,q)}\right] \quad (10)$$

and for insulators:

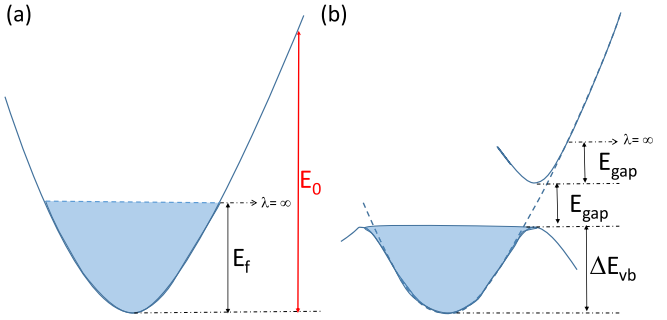

Fig. 5. Energy diagram for an electron interacting in (a) a metal and (b) an insulator. For a metal $\lambda = \infty$ at the Fermi level, as no empty states are available for the projectile to scatter into. For insulators $\lambda = \infty$ if the energy is E_{gap} above the conduction-band minimum as at least this amount of energy is required to create an electron–hole pair.

$$1/\lambda = \int_0^{E_0-(\Delta E_{vb}+E_{gap})} W_b(\omega, E_0)d\omega = \int_0^{E_0-(\Delta E_{vb}+E_{gap})} \frac{d\omega}{\pi E_0}\int_{q_-}^{q_+}\frac{dq}{q}\,\mathrm{Im}\left[\frac{-1}{\epsilon(\omega,q)}\right] \quad (11)$$

If $\mathrm{Im}[-1/\epsilon(\omega,q)]$ is zero for $\omega < E_{gap}$ (as required for the dielectric function of an insulator) the smallest projectile energy for which excitations can occur is $E_0 = \Delta E_{vb} + 2E_{gap}$. For the metallic model E_F, the Fermi energy, is taken to be that of a free electron gas with a plasmon energy of 15 eV (i.e. 10.9 eV), and for the insulator ΔE_{vb}, the width of the valence band, is approximated by the Fermi energy of an electron gas with half the density of our metal model (i.e. $\Delta E_{vb} = 6.9$ eV) and $E_{gap} \approx U = 11$ eV.

Now we want to consider the situation at lower energies, around the E_0 values where the IMFP λ has a minimum. We choose for E_0 values of 25, 40 and 70 eV and consider again the dielectric functions of Table 1. Now the deeper level cannot be excited. In Fig. 6 the lower limit of the integration of the DIIMFP as well as the dispersion are shown as a function of the energy loss. The lower the projectile energy the larger the minimum momentum

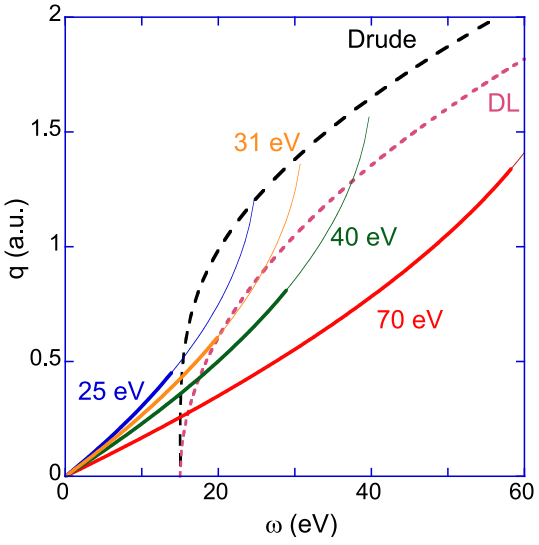

Fig. 6. Lower Limit of the q integration as a function of energy loss for incoming energies as indicated. The thin part of these curves do not contribute to the DIIMFP, as there the final state is occupied (i.e. within the Fermi sphere). The plasmon dispersion (dashed lines) in the DL model and Drude model is shown as well.

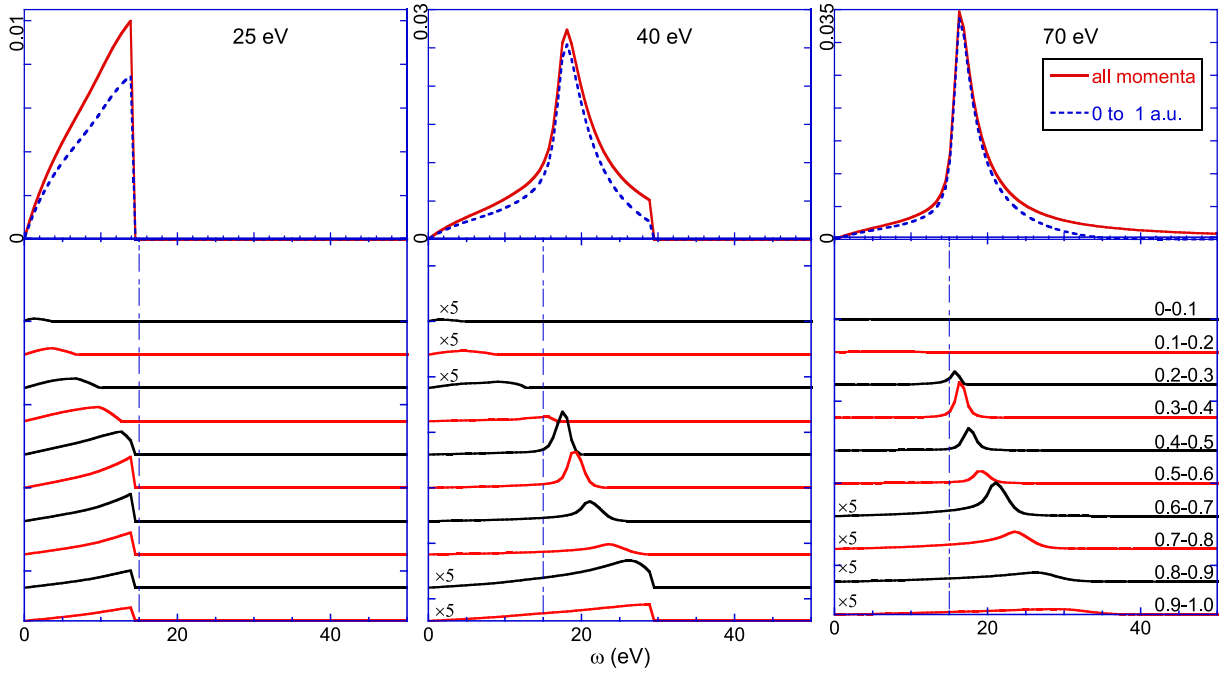

Fig. 7. Similar figure as Fig. 3 but now for (metal) Mermin dielectric function and E_0 values of 25, 40 and 70 eV. All E_0 values are relative to the bottom of the conduction band. Subtract 10.9 from E_0 to get the incoming energies relative to the Fermi level.

transfer for a given ω value. For $E_0 = 25$ eV the curves for the lower limit of the integration and plasmon dispersion never cross. All intensity in the partial DIIMFP at a certain q value is thus due to the wings of the plasmon peak extending towards $\omega = 0$. At $E_0 = 40$ eV the lower limit of the integration crosses the dispersion curve for the Drude model, but only just approaches it for the DL model. We expect here the partial DIIMFP near $q = 0.7$ to be much larger for the Drude model than for the DL model. At $E_0 = 70$ eV the situation becomes more similar to that shown in Fig. 4 with the q_- curve crossing both dispersion curves at relatively small q values.

As a consequence the partial DIIMFP plots at these energies look completely different. We show them only for the Mermin model (Fig. 7). For $E_0 = 25$ eV the partial DIIMFP curves show a gradual rise, followed by a steep decline for ω values were the corresponding minimum momentum transfer approaches the upper limit of the momentum bin. Here the peaks in the partial DIIMFP are not related to any structure in the loss function, but a consequence of the dependence of q_- on ω. At 40 eV one observes again peaks near the nominal plasmon energy value (but only for q values larger than 0.4 a.u.). At 70 eV the plots resemble those at 40 eV, except that the plasmon peak appears in the partial DIIMFP at lower q values (0.2 a.u.).

We calculated the IMFP as well for the other model dielectric functions for a range of E_0 values as shown in Fig. 8. Above 60 eV all models give a similar IMFP, but at lower energies, the differences are distinct. For the lower incoming energies the incoming electron cannot excite the plasmon anymore. This causes the increase in the IMFP with decreasing E_0. For the DL dielectric function this increase starts already when E_0 is reduced below 40 eV as here the dispersion affects the energy of the plasmon most. For the Drude dielectric function, with less dispersion the IMFP starts only increasing when E_0 is reduced below 30 eV. Finally, the Mermin loss function has a minimum in the DIIMFP at a similar E_0 value as the DL dielectric function, but the increase when E_0 is reduced below this value is much slower. This is because the increased broadening in the Mermin loss function, away from $q = 0$, causing additional intensity in the partial DIIMFP near $\omega = 0$.

This is illustrated in Fig. 9 for the partial DIIMFP between 0.4 and 0.5 a.u., where the differences are most pronounced. At $E_0 = 25$ eV the DL partial DIIMFP has the smallest area, 4 times smaller than the Mermin one. This is due to the additional broadening of the Mermin loss function away from $q = 0$. For the Drude model the q_- line for $E_0 = 25$ eV approaches the plasmon dispersion line for $q \simeq 0.5$ a.u. (see Fig. 6) and hence its partial DIIMFP becomes already large for $q \approx 0.5$, resulting in much smaller IMFP for the Drude model at these E_0 values compared to DL. At $E_0 = 31$ eV the q_- line crosses the dispersion curve for the Drude model and excitation of the plasmon becomes possible, resulting in a huge peak in the partial DIIMFP near $\omega = 15$ eV, whereas for the DL (and Mermin) model the q_- line only approaches the dispersion curve. Thus the IMFP at 31 eV is much shorter for the Drude model, and longest for the DL one. At $E_0 = 40$ eV plasmon excitation becomes possible for all models and both the IMFP and area of the partial DIIMFP becomes more similar, but the different peak position in the DIIMFP still reflects the difference in dispersion.

Similar calculations of the mean free path were done for the insulator dielectric functions of Table 2. As these dielectric functions corresponds to half the electron density compared to the metallic one, the obtained IMFP at high energies is about twice as large. At energies below 70 eV there were again significant differences between the 4 models. Now the difference between the Drude and DL dielectric function was less pronounced as their dispersion is now more similar (as the influence of A_i on the peak position: $\sqrt{A_i + \omega_i(q)^2}$ is now less dominant for low q values). The MLL loss function has a reduced intensity in the gap region compared to the Mermin loss function (see Ref. [12] for examples). Thus the IMFP at very low energies is larger for the MLL case compared to the Mermin case, but is still considerable smaller than for the Drude and DL models.

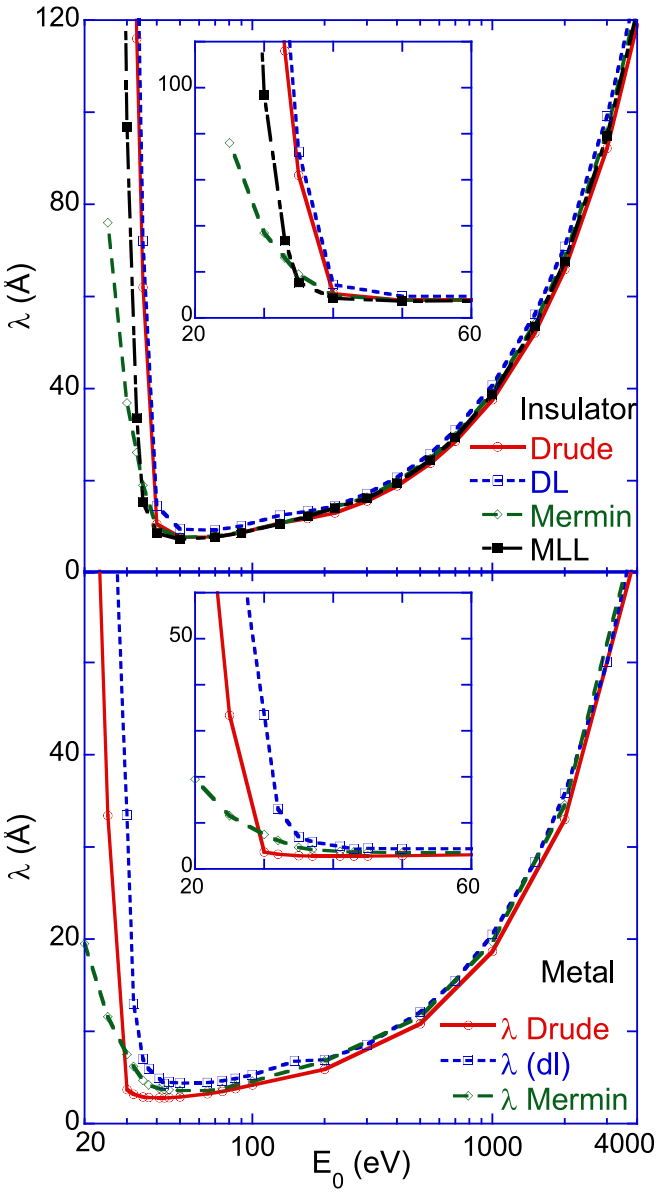

Fig. 8. The IMFP corresponding to the four different functional forms of the dielectric function for an insulator (top) and three different forms for a metal (bottom). Projectile energies E_0 are relative to the bottom of the band (see Fig. 5). For the metal subtract 10.9 eV to get energies relative to the Fermi level. For the insulator subtract 17 eV to get energy relative to bottom conduction band. The inserts show the low energy part on an expanded (linear) scale.

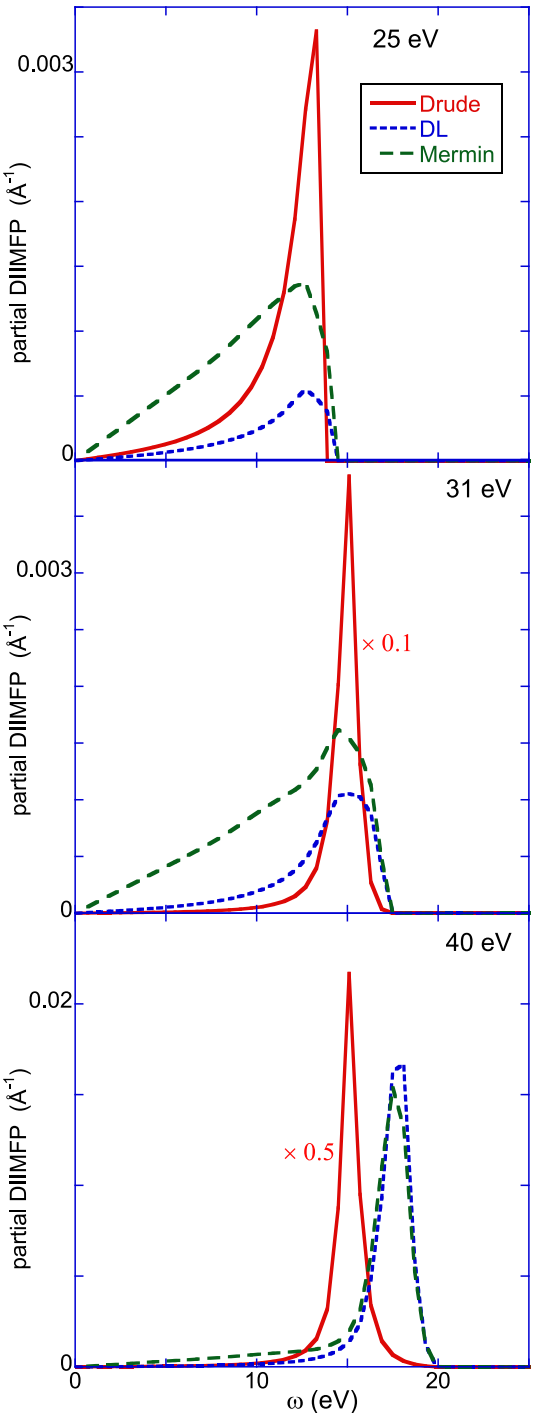

Fig. 9. The partial DIIMFP for $0.4 < q < 0.5$ for E_0 equal to 25, 31 and 40 eV (relative to bottom valence band) for the three different model dielectric functions of Table 1. The Drude intensity at 31 and 40 eV is multiplied by 0.1 and 0.5 respectively.

5. Proton stopping and straggling

We can use Eq. (10) for protons as well, if we replace $1/E_0$ by $2/v^2$. The protons will not be affected by the Fermi exclusion principle, so we can replace $E_0 - E_f$ by simply E_0.

The energy resolution in ion beam experiments is not good enough to resolve the energy loss due to a single energy loss event and hence the IMFP of protons cannot be measured directly. The quantity considered in this field is usually the (average) energy loss per unit distance traveled (dE/dx) i.e. the stopping force. It can be calculated based on the DIIMFP as $W_b(\omega, E_0)$ is the probability that there is a collision with energy loss ω per unit path length. Such a collision contributes ω to the energy loss. One obtains thus the stopping dE/dx if one integrates the energy-weighted DIIMFP over all possible energy losses:

$$\frac{dE}{dx} = \int_0^{E_0} \omega W_b(\omega, E_0) d\omega = \int_0^{E_0} \frac{\omega d\omega}{\pi E_0} \int_{q_-}^{q_+} \frac{dq}{q} \mathrm{Im}\left[\frac{-1}{\epsilon(\omega, q)}\right] \qquad (12)$$

In line with this definitions we will refer to the energy-weighted DIIMFP as $\frac{d^2E}{dxd\omega}$.

For a given energy loss value the limit of integration over momentum ($q_\pm$) in Eq. (12) depends on ω. Now one can interchange the order of integration. Then the limits of the accessible

energy losses will depend on q, as explained in Fig. 2(b), and extends from 0 to qv.

$$\frac{dE}{dx} = \frac{2}{\pi v^2}\int_0^{\infty}\frac{dq}{q}\int_0^{qv}\omega\, d\omega\, \mathrm{Im}\left[\frac{-1}{\epsilon(\omega,q)}\right] \tag{13}$$

This is the usual equation for ion stopping in terms of the dielectric function. To highlight the importance of the DIIMFP, in the context of ion stopping we will continue using Eq. (12) rather than Eq. (13).

Besides the replacement of $1/E_0$ by $2/v^2$ the outcome of Eq. (12) differs from the electron case via the integration limits $q_{\pm}$ which depend on the projectile mass, see Eq. (9). In Fig. 10 we show the development of q_- with energy loss for protons with energy of 20, 60 and 600 keV as well as the plasmon dispersion. This figure is rather similar to Fig. 6 except that the relevant projectile energies are three orders of magnitude larger. Again, inelastic excitations will be strong only if the q_- curve is to the right of the plasmon dispersion curve. However, now there are two crossings of the q_- line and the plasmon dispersion. The second crossing corresponds approximately to the maximum energy transfer for a proton scattering from a stationary electron ($4\frac{m}{M}E_0$). This means that for protons there is hardly any intensity in the partial DIIMFP at both very low and very high q values (e.g. $q < 0.4$ or $q > 2.7$ a.u. for $E_0 = 60$ keV).

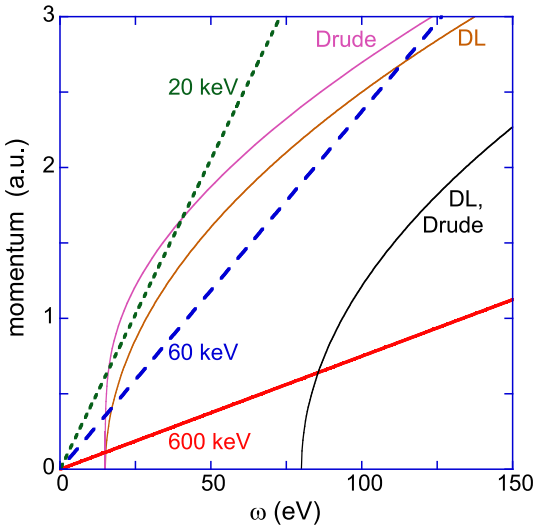

Fig. 10. Plots of q_- for protons as a projectile at 20 keV, 60 keV and 600 keV (thick lines) as well as the dispersion of the 15 and 80 eV level in both the Drude and DL model (thin lines).

As an example we show the partial DIIMFP curves for protons and the Mermin and MLL dielectric function, both for insulators (see Table 2) in Fig. 11. The 80 eV level is not visible for $E_0 = 20$ keV and 60 keV (as the corresponding q_- line does not cross the dispersion curve of that level, see Fig. 10), and hence this level will not contribute to the energy loss at these energies (in spite of the fact that the actual kinetic energy of the protons is far in excess of 80 eV), but it can be observed at larger q values for $E_0 = 600$ keV. Integrating the DIIMFP over all energies one obtains the IMFP of protons which are reproduced in Fig. 12, top panel. A proton has a similar IMFP as an electron with the same velocity. The differences in the mean free path of protons for the different models at low energies appears now somewhat larger, as the q_- lines extends further for protons than for electrons (see Fig. 6 and Fig. 10). If one disregards the Pauli exclusion principle the differences in the IMFP is larger for electrons as well.

In Fig. 10 the dispersion of the 80 eV level was described using $\alpha_2 = 1$. If one would take $\alpha_2 = 0.1$ then there would be a crossing of the q_- line (at a rather large q value) and this would change the calculated stopping hugely. Hence we kept $\alpha_2 = 1$ in the proton stopping calculations. Compared to the DIIMFP itself $\frac{d^2E}{dxd\omega}$ has a larger fraction of its area at larger energy losses, and a larger fraction from

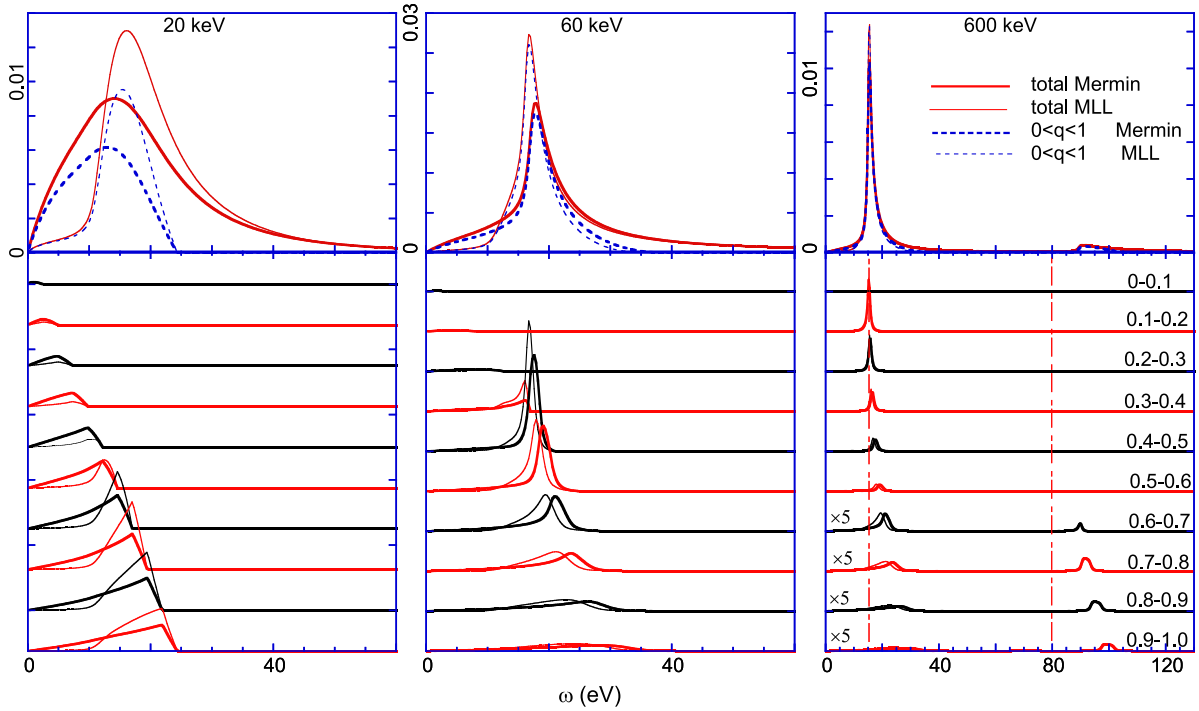

Fig. 11. Similar plot to Fig. 3 but now for protons as projectiles and the Mermin loss function for an insulator (thick lines) and the MLL loss function (thin lines). The 80 eV level is not excited by 20 keV or 60 keV protons, hence the energy scale was expanded in these cases.

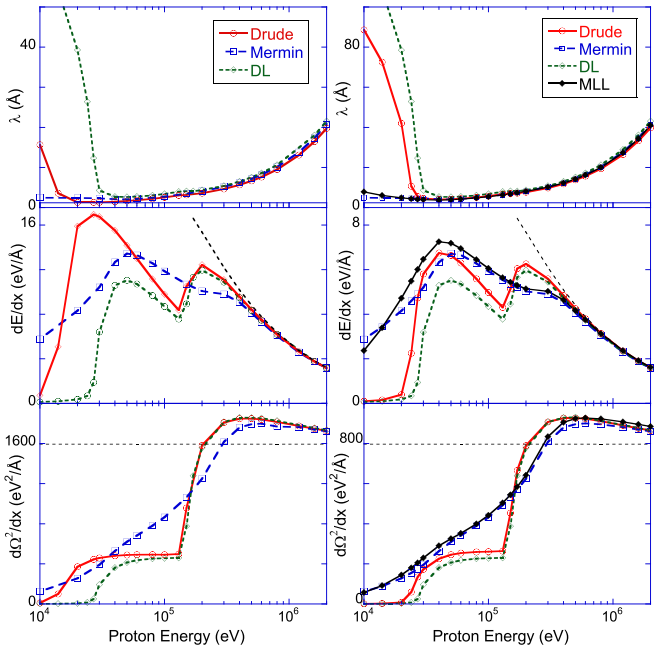

Fig. 12. The IMFP (top), stopping force (middle) and straggling per unit pathlength (bottom) for protons and the three metal dielectric functions (left panels) and insulator dielectric function (right panels). The thin black dashed lines correspond tot the Bethe limit (stopping) and the Bohr high-energy limit of the straggling ($(d\Omega^2/dx)_{\text{Bohr}} = 4\pi N$ with N the electron density.)

its intensity originates from collisions with larger q values. This is illustrated in Fig. 13. For the DIIMFP the contribution of the 80 eV level is at 500 keV 20 times less intense than the 15 eV level. For $\frac{d^2E}{dxd\omega}$ its intensity is only 3 times less. Thus, as is well known, the deeper levels, that only play a minor role in the calculation of the IMFP, have a more significant influence on the ion stopping.

The resulting stopping forces are shown in Fig. 12 for both the metal and insulator dielectric function. At high projectile energies all models give similar stopping values, but at lower and intermediate E_0 values, there are significant differences. Again the extra broadening away from $q = 0$ of the Mermin and MLL dielectric functions causes an increase of the projectile–target interaction at lower E_0 values.

For the Drude and DL model the turn on of the 'core electron contribution' with increasing E_0 values is quite sudden and causes a second maximum in the stopping. For the Mermin and MLL loss function the broadening at the q value where q_- crosses the dispersion curve of the deeper curve is significant and, as a consequence the core level contribution kicks in more gradually, changing the second peak into a shoulder. This is illustrated in Fig. 13 as well. For the DL case there is no sign of the 80 eV level in the DIIMFP at 100 keV, whereas for the Mermin case it contributes and causes a small shoulder in the DIIMFP centered somewhat above 100 eV energy loss, and this shoulder contributes more significantly to $\frac{d^2E}{dxd\omega}$. The more gradual increase of the core levels with increasing E_0 is also seen in the experiment for Al [42] and is clear evidence of the quantum-based models are more appropriate for the description of ion stopping than the classical-physics based models.

If one weights the DIIMFP with ω^2 and integrates over ω one obtains the straggling per unit length traveled: $d\Omega^2/dx$:

$$\frac{d\Omega^2}{dx} = \int_0^{E_0} \omega^2 W_b(\omega, E_0) d\omega = \int_0^{E_0} \frac{\omega^2 d\omega}{\pi E_0} \int_{q_-}^{q_+} \frac{dq}{q} \operatorname{Im}\left[\frac{-1}{\epsilon(\omega, q)}\right]. \quad (14)$$

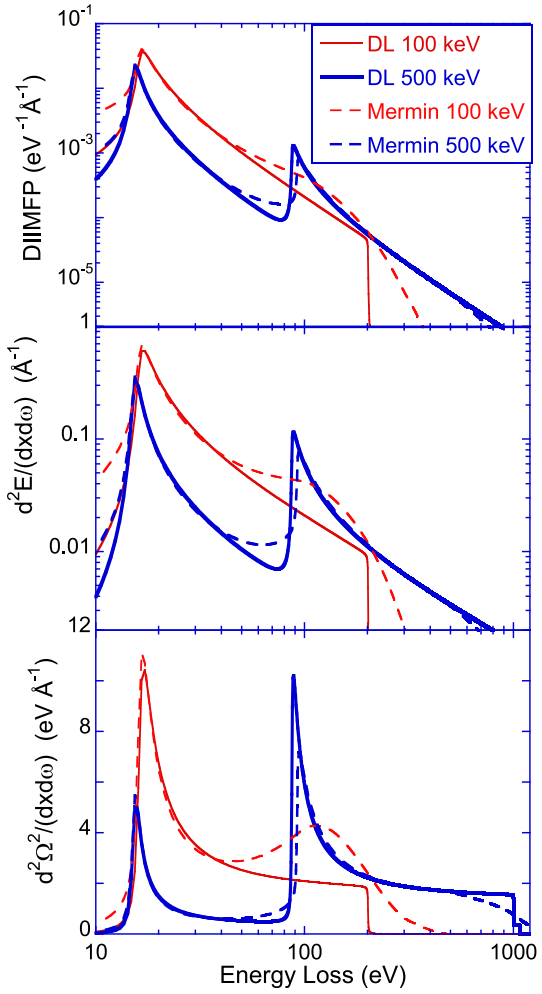

Fig. 13. The DIIMFP itself (top) and the DIIMFP weighted by the energy loss (central) and energy loss square (bottom) for 100 and 500 keV protons. for the (metal) Mermin and DL dielectric function.

Thus the DIIMFP weighted by ω^2 corresponds to $\frac{d^2\Omega^2}{dxd\omega}$. As the weighting is now with ω^2 the contribution of the 80 eV level to the straggling is even more important (see Fig. 13, lower panel) and it dominates the valence band contribution for higher E_0 values (as it contains more electrons). In Fig. 12, lower panel, we show the straggling per unit length, $d\Omega^2/dx$, as a function of proton energy for the different dielectric functions. The Drude and DL dielectric function show a sharp increase in $d\Omega^2/dx$ when the 80 eV level start contributing to the DIIMFP. Again this happens at relatively large q values and at these q values the Mermin and MLL loss functions are very broad. Thus the contribution of the 80 eV level to the straggling increases also much more gradually with the proton energy for these models.

6. Limitations of the these approaches to describe deeper levels

In the previous we used several empirical models to describe the level at 80 eV. At these energies maxima in the loss level will be usually due to a semi-core level. For such levels solid state effects are minor and an atomic description is probably more appropriate. For this reason it has become customary to describe deeper levels by in terms of Generalized Oscillator Strength (GOS) (per unit energy loss) $df(\omega, q)/d\omega$ which is usually

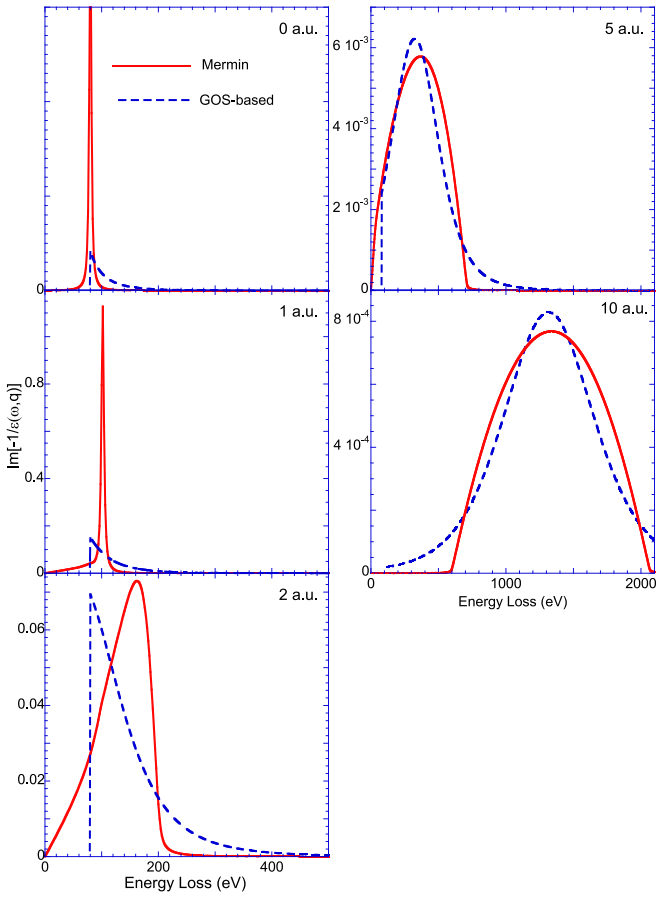

Fig. 14. A comparison of the Mermin loss function ($\omega = 80$ eV, $\gamma = 4$ eV) and GOS distribution at selected q values. The GOS curve were calculated for a 1s level at 80 eV binding energy and $Z = 3.35$ value (as for this notional Z value the 1s binding energy would be close to 80 eV).

calculated based on hydrogenic wave functions [10,43]. The contribution of the core level to the dielectric function is then given by:

$$\mathrm{Im}\left[\frac{-1}{\epsilon(\omega,q)}\right] = \frac{2\pi^2 N_a}{\omega}\frac{df(\omega,q)}{d\omega}, \tag{15}$$

with N_a the atomic density.

To get some insight in the level of differences between these approaches we compare in Fig. 14 the contribution to the Mermin loss function of the 80 eV component with the calculated distribution from the GOS at selected q values. Both curves are normalized so they correspond to the same electron density. The width of the Mermin loss function in the optical limit relates to the relaxation time of the plasmon, but is in practice a fitting parameter. The width of the GOS is a consequence of the hydrogenic wave functions. At high q values both approaches have a maximum at the Bethe ridge, but the Mermin distribution resembles (for modest Γ values) an inverted parabola and the GOS derived loss function has a more gradually-decreasing intensity away from the Bethe ridge. The GOS-derived loss function is strictly 0 for energies below the core level, whereas the Mermin loss function, especially at intermediate q values, extends to lower losses. As a consequence, when using the Mermin approach, the core level starts contributing to the stopping and straggling at a lower projectile energy, as can be seen in Fig. 13 for the Mermin DIIMFP at 100 keV. The MLL approach (using $U = 11$ eV) would give very similar results as the Mermin approach as near 80 eV the influence of U on $\sqrt{U^2+\omega^2}$ is minor.

7. Discussion and conclusion

We have illustrated that for a given loss function in the optical limit one can obtain different estimates of quantities such as the DIIMFP, IMFP and proton stopping and straggling depending on how the model one adopts describes $\epsilon(\omega,q)$ away from $q = 0$. These differences tend to be larger if the projectile energy is lower and these differences are more pronounced for stopping and straggling.

We have shown that insight in these calculations can be obtained by studying the partial DIIMFP, and by comparing the energy loss dependence of the q_- values with the plasmon dispersion. At low projectile energies the magnitude of the tail of the loss function extending at a given q value towards $\omega = 0$ determines effectively the IMFP and proton stopping. However, the dispersion has a significant influence on the energy below which the IMFP starts to increase.

In this work we used for the Drude and DL model a very rudimentary model describing the dispersion (simple quadratic dispersion). One could certainly improve on this by replacing Eq. (3) with:

$$\omega_i(q)^2 = \omega_i(0)^2 + \beta q^2 + q^4/4 \tag{16}$$

Here the $q^4/4$ term ensures that the dispersion will follow the Bethe ridge at very large q values, whereas the β parameter can be either determined from the plasmon dispersion in free electron gas theory ($\beta = \frac{1}{3}\left(\frac{3\pi}{4}\right)^{1/3}\omega_i(0)^{2/3}$ [17]) or adjusted to match the experimental dispersion as observed in transmission EELS experiments. For example, for Cs the dispersion at small q values is known to be negative [44]. Here the main aim was to explore how dispersion affects the IMFP and proton stopping/straggling, rather than to establish what the appropriate dispersion behavior is.

There is a very strong (reciprocal) correspondence between the behavior of the stopping for E_0 values near the stopping force maximum and the inelastic mean free path for E_0 values near the IMFP minimum. In fact one can calculate the inelastic mean free path for protons near the stopping force maximum, and it is very similar to that of electrons at the IMFP minimum. The energy of the stopping force maximum is $\simeq 1836\times$ (i.e. the proton mass) larger than the energy of the IMFP minimum. Around the stopping force maximum there are many more reliable data available for the stopping than for the IMFP near its minimum, where the best data appear to come from the analysis of X-ray absorption measurements [45]. A dielectric function that describes the experimental proton stopping force data well is expected to be a good candidate for the calculation of the electron IMFP. However, at small proton velocities it is well-established that non first-Born contributions are significant [46,47] and similar deviations are expected for electrons.

It is thus not possible to be confident that one gets the right estimate of the IMFP, stopping and straggling if one determines the dielectric function such that it describes the loss function in the optical limit well. More restraints are required to make sure that the momentum dependence of the dielectric function is described well. One possible way forward would be to fit not only the loss function at $q = 0$ but also the loss function in the limit of high q. Here the loss function becomes a Compton profile, for which many measurements are available [48].

Acknowledgement

This work was made possible by funding of the Australian Research Council and the Brazilian Agencies CNPq and FAPERGS. We are also thankful to Nestor Arista for reading the manuscript.

Appendix A. Appendix

For completeness we reproduce here the formula for the Lindhard [21] and Levine–Louie (LL) [28] dielectric function.

The Lindhard dielectric function for an electron gas with density n can be expressed in terms of the Fermi velocity v_f (or Fermi energy $E_f = \frac{1}{2}v_f^2$) and the dimensionless variables $u = \omega/(qv_f)$, $z = q/(2v_f)$and $\chi^2 = 1/(\pi v_f)$ according to

$$\epsilon^L(\omega,q) = 1 + \frac{\chi^2}{z^2}(f_1(u,z) + if_2(u,z)) \tag{17}$$

where

$$f_1(u,z) = \frac{1}{2} + \frac{1}{8z}(g(z-u) + g(z+u)) \tag{18}$$

with

$$g(x) = (1-x^2)\ln\left|\frac{1+x}{1-x}\right| \tag{19}$$

and

$$f_2(u,z) = \frac{\pi}{2}u\Theta(1-z-u) + \frac{\pi}{8z}(1-(z-u)^2)\Theta(1-|z-u|)\Theta(z+u-1) \tag{20}$$

where $\Theta(x)$ is the usual step function.

The LL dielectric function is obtained by introducing a gap energy U in the imaginary part of the Lindhard dielectric function according to

$$\epsilon_2^{LL}(\omega,q) = \epsilon_2^L(\omega_-,q)\Theta(|\omega|-U) \tag{21}$$

with $\omega_- = \sqrt{\omega^2 - U^2}$. The real part of the LL dielectric function can be obtained straightforwardly from Kramers–Krönig relation and reads

$$\epsilon_1^{LL}(\omega,q) = \epsilon_1^L(\omega_-,q)\Theta(|\omega|-U) + \left(1 + \frac{2}{\pi v_f}F(Q,\Delta)\right)\Theta(U-|\omega|) \tag{22}$$

and

$$F(Q,\Delta) = \frac{1}{Q^2} - \frac{\Delta}{2Q^3}\left(\arctan\frac{2Q+Q^2}{\Delta} + \arctan\frac{2Q-Q^2}{\Delta}\right) + \left(\frac{\Delta^2}{8Q^5} + \frac{1}{2Q^3} - \frac{1}{8Q}\right)\ln\left(\frac{\Delta^2 + (2Q+Q^2)^2}{\Delta^2 + (2Q-Q^2)^2}\right) \tag{23}$$

with $Q = q/v_f$ and $\Delta^2 = (U^2 - \omega^2)/E_f^2$.

References

[1] P.E. Batson, J. Silcox, Experimental energy-loss function, $Im\left[\frac{-1}{\epsilon(\omega,q)}\right]$, for aluminum, Phys. Rev. B 27 (1983) 5224–5239, http://dx.doi.org/10.1103/PhysRevB.27.5224.

[2] J. Sprösser-Prou, A. vom Felde, J. Fink, Aluminum bulk-plasmon dispersion and its anisotropy, Phys. Rev. B 40 (1989) 5799–5801, http://dx.doi.org/10.1103/physrevb.40.5799.

[3] N. Watanabe, H. Hayashi, Y. Udagawa, Bethe surface of liquid water determined by inelastic x-ray scattering spectroscopy and electron correlation effects, Bull. Chem. Soc. Jpn. 70 (1997) 719, http://dx.doi.org/10.1246/bcsj.70.719.

[4] G. Onida, L. Reining, A. Rubio, Electronic excitations: density-functional versus many-body green's-function approaches, Rev. Mod. Phys. 74 (2002) 601, http://dx.doi.org/10.1103/revmodphys.74.601.

[5] E.D. Palik, Handbook of Optical Constants of Solids II, Academic Press, New York, 1991.

[6] D. Penn, Electron mean-free-path calculations using a model dielectric function, Phys. Rev. B 35 (1987) 482–486, http://dx.doi.org/10.1103/PhysRevB.35.482.

[7] P. Sigmund, Stopping of Heavy Ions - A Theoretical Approach, first edition., Springer, Berlin Heidelberg New York, 2004, ISBN 3 540 22273 1.

[8] H. Shinotsuka, B. Da, S. Tanuma, H. Yoshikawa, C.J. Powell, D.R. Penn, Calculations of electron inelastic mean free paths. XI. Data for liquid water for energies from 50eV to 30keV, Surf. Interface Anal. 49 (2016) 238, http://dx.doi.org/10.1002/sia.6123.

[9] H. Nikjoo, D. Emfietzoglou, T. Liamsuwan, R. Taleei, D. Liljequist, S. Uehara, Radiation track, DNA damage and response—a review, Rep. Prog. Phys. 79 (2016) 116601, http://dx.doi.org/10.1088/0034-4885/79/11/116601.

[10] R.F. Egerton, Electron Energy-loss Spectroscopy in the Electron Microscope, Plenum Press, New York, 1996.

[11] H. Raether, Excitation of plasmons and interband transitions by electrons, Springer Tracts in Modern Physics, vol. 88, Springer Verlag, Berlin, 1979.

[12] M. Vos, P.L. Grande, Simple model dielectric functions for insulators, J. Phys. Chem. Solids 104 (2017) 192, http://dx.doi.org/10.1016/j.jpcs.2016.12.015.

[13] M. Vos, P.L. Grande, Extracting dielectric function from high-energy REELS measurements, Surf. Interface Anal. (2017), http://dx.doi.org/10.1002/sia.6227 (in press).

[14] C. Tung, Y. Chen, C. Kwei, T. Chou, Differential cross sections for plasmon excitations and reflected electron-energy-loss spectra, Phys. Rev. B 49 (1994) 16684–16693, http://dx.doi.org/10.1103/PhysRevB.49.16684.

[15] C.M. Kwei, Y.F. Chen, C.J. Tung, J.P. Wang, Electron inelastic mean free paths for plasmon excitations and interband transitions, Surf. Sci. 293 (1993) 202, http://dx.doi.org/10.1016/0039-6028(93)90314-a.

[16] W.S.M. Werner, K. Glantschnig, C. Ambrosch-Draxl, Optical constants and inelastic electron-scattering data for 17 elemental metals, J. Phys. Chem. Ref. Data 38 (2009) 1013–1092, http://dx.doi.org/10.1063/1.3243762.

[17] R.A. Ferrell, Characteristic energy loss of electrons passing through metal foils. II. Dispersion relation and short wavelength cutoff for plasma oscillations, Phys. Rev. 107 (1957) 450, http://dx.doi.org/10.1103/physrev.107.450.

[18] R.H. Ritchie, A. Howie, Electron excitation and the optical potential in electron microscopy, Philos. Mag. 36 (1977) 463, http://dx.doi.org/10.1080/14786437708244948.

[19] F. Yubero, J. Sanz, B. Ramskov, S. Tougaard, Model for quantitative analysis of reflection-electron-energy-loss spectra: Angular dependence, Phys. Rev. B, 1095-3795 (1996) 9719, http://dx.doi.org/10.1103/physrevb.53.9719.

[20] S. Hajati, O. Romanyuk, J. Zemek, S. Tougaard, Validity of Yubero-Tougaard theory to quantitatively determine the dielectric properties of surface nanofilms, Phys. Rev. B 77 (2008) 155403, http://dx.doi.org/10.1103/physrevb.77.155403.

[21] J. Lindhard, K. Dan, Vidensk. Selsk. Mat.-Fys. Medd. 28 (8) (1954), URL http://gymarkiv.sdu.dk/MFM/kdvs/mfm%2020-29/mfm-28-8.pdf.

[22] N. Mermin, Lindhard dielectric function in the relaxation-time approximation, Phys. Rev. B 1 (1970) 2362–2363, http://dx.doi.org/10.1103/physrevb.1.2362.

[23] I. Abril, R. Garcia-Molina, C. Denton, F.J. Pérez-Pérez, N. Arista, Dielectric description of wakes and stopping powers in solids, Phys. Rev. A, 1094-1622 58 (1998) 357, http://dx.doi.org/10.1103/physreva.58.357.

[24] S.P. Limandri, R.C. Fadanelli, M. Behar, L. Nagamine, J.M. Fernandez-Varea, I. Abril, R. Garcia-Molina, C. Montanari, J. Aguiar, D. Mitnik, J.E. Miraglia, N.R. Arista, Stopping cross sections of TiO_2 for H and He ions, Eur. Phys. J. D 68 (2014) 194, http://dx.doi.org/10.1140/epjd/e2014-40782-6.

[25] C.D. Denton, I. Abril, R. Garcia-Molina, J.C. Moreno-Mańn, S. Heredia-Avalos, Influence of the description of the target energy-loss function on the energy loss of swift projectiles, Surf. Interface Anal. 40 (2008) 1481, http://dx.doi.org/10.1002/sia.2936.

[26] B. Da, H. Shinotsuka, H. Yoshikawa, Z.J. Ding, S. Tanuma, Extended mermin method for calculating the electron inelastic mean free path, Phys. Rev. Lett., 1079-7114 113 (2014) 063201, http://dx.doi.org/10.1103/physrevlett.113.063201.

[27] D.J. Planes, R. Garcia-Molina, N.R. Abril, I. Arista, Wavenumber dependence of the energy loss function of graphite and aluminium, J. Electron Spectrosc. Relat. Phenom, 0368-2048 82 (1996) 23, http://dx.doi.org/10.1016/s0368-2048(96)03043-5.

[28] Z.H. Levine, S.G. Louie, New model dielectric function and exchange-correlation potential for semiconductors and insulators, Phys. Rev. B 25 (1982) 6310, http://dx.doi.org/10.1103/physrevb.25.6310.

[29] C.D. Archubi, N.R. Arista, A comparative study of threshold effects in the energy loss moments of protons, electrons and positrons using dielectric models for band-gap materials, The European Physical Journal B 90 (2017), http://dx.doi.org/10.1140/epjb/e2016-70637-9.

[30] S. Tanuma, C.J. Powell, D.R. Penn, Calculations of electron inelastic mean free paths, Surf. Interface Anal. 37 (2005) 1–14, http://dx.doi.org/10.1002/sia.1997.

[31] A. Howie, Inelastic scattering of electrons by crystals I. The theory of small-angle inelastic scattering, Proc. Royal Soc. London, A 271 (1963) 268–287.

[32] D. Emfietzoglou, I. Kyriakou, R. Garcia-Molina, I. Abril, H. Nikjoo, Inelastic cross sections for low-energy electrons in liquid water: exchange and correlation effects, Radiat. Res. 180 (2013) 499, http://dx.doi.org/10.1667/rr13362.1.

[33] M. Dapor, G. Garberoglio, L. Calliari, Energy loss of electrons impinging upon glassy carbon, amorphous carbon, and diamond: comparison between two different dispersion laws, Nucl. Instrum. Methods Phys. Res., Sect. B 352 (2015) 181, http://dx.doi.org/10.1016/j.nimb.2014.11.115.

[34] J.D. Bourke, C.T. Chantler, Momentum-dependent lifetime broadening of electron energy loss spectra: a self-consistent coupled-plasmon model, J. Phys. Chem. Lett., 1948-7185 6 (2015) 314, http://dx.doi.org/10.1021/jz5023812.

[35] W.S.M. Werner, Differential surface and volume excitation probability of medium-energy electrons in solids, Phys. Rev. B 74 (2006) 075421, http://dx.doi.org/10.1103/PhysRevB.74.075421.

[36] R.H. Ritchie, Plasma losses by fast electrons in thin films, Phys. Rev. 106 (1957) 874–881, http://dx.doi.org/10.1103/PhysRev. 106.874.
[37] S. Tougaard, F. Yubero, QUEELS-$\epsilon(k,\omega)$ REELS user guideversion 3.03, 2011.
[38] M. Vos, P.L. Grande, The relation between the electron energy loss spectra of hafnia and its dielectric function, Surf. Sci. 630 (2014) 1–8, http://dx.doi.org/10.1016/j.susc.2014.06.008.
[39] D. Emfietzoglou, I. Kyriakou, R. Garcia-Molina, I. Abril, The effect of static many-body local-field corrections to inelastic electron scattering in condensed media, J. Appl. Phys. 114 (2013) 144907, http://dx.doi.org/10.1063/1.4824541.
[40] D. Emfietzoglou, I. Kyriakou, R. Garcia-Molina, I. Abril, Inelastic mean free path of low-energy electrons in condensed media: beyond the standard models, Surf. Interface Anal. 49 (2017) 4, http://dx.doi.org/10.1002/sia.5878.
[41] F. Flores, Dynamical interaction of charges with condensed matter, Interaction of Charged Particles with Solids and Surfaces, volume NATO ASI Series B, Plenum Press, New York, 1991, p. 3.
[42] J.F. Ziegler, J.P. Biersack, U. Littmark, The Stopping and Range of Ions in Solids, Pergamon Press, New York, 1985.
[43] S. Heredia-Avalos, R. Garcia-Molina, J.M. Fernández-Varea, I. Abril, Calculated energy loss of swift he, li, b, and n ions in SiO_2, Al_22O_3, and ZrO_2, Phys. Rev. A 72 (2005) 052902, http://dx.doi.org/10.1103/physreva.72.052902.
[44] A. vom Felde, J. Sprösser-Prou, J. Fink, Valence-electron excitations in the alkali metals, Phys. Rev. B 40 (1989) 10181–10193, http://dx.doi.org/10.1103/PhysRevB.40.10181.
[45] J.D. Bourke, C.T. Chantler, Measurements of electron inelastic mean free paths in materials, Phys. Rev. Lett. 104 (206601) (2010), http://dx.doi.org/10.1103/physrevlett.104.206601.
[46] P.M. Echenique, R.M. Nieminen, R.H. Ritchie, Density functional calculation of stopping power of an electron gas for slow ions, Solid State Commun., 0038-1098 37 (1981) 779, http://dx.doi.org/10.1016/0038-1098(81)91173-X.
[47] P.M. Echenique, R.M. Nieminen, J.C. Ashley, R.H. Ritchie, Nonlinear stopping power of an electron gas for slow ions. Phys. Rev. A 33 (1986) 904, http://dx.doi.org/10.1103/physreva.33.897.
[48] M. Vos, A model dielectric function for low and very high momentum transfer, Nuclear Instruments & MethodsB 366 (2015) 6, http://dx.doi.org/10.1016/j.nimb.2015.09.091.